energy&fuels

pubs.acs.org/EF Article

Pore Structure and Compressibility Characteristics of Heat-Treated Coals by N_2 Adsorption/Desorption and Mercury Intrusion Porosimetry

Zhentao Li, Dameng Liu,* Yidong Cai, Guangyao Si, and Yunpeng Wang

Cite This: *Energy Fuels* 2020, 34, 3173−3187

Read Online

ACCESS | Metrics & More | Article Recommendations

ABSTRACT: To improve the physical properties of a coal reservoir with heat treatment and enhance the coalbed methane recovery, the characteristics of gas generation and pore structure evolution of different rank coals during heat treatment were investigated by combining the thermogravimetry−mass spectrometry, N_2 adsorption/desorption, and mercury intrusion porosimetry analyses. The impacts of these characteristics on pore compressibility were also studied. The results indicate that the macromolecular organic matter in coals begins to decompose into hydrocarbon gases (such as CH_4 and C_2H_4) at temperature ranging from 350 to 600 °C, and then the production peaks of CO and CO_2 exist at 600−800 °C in different rank coals and are accompanied by the generation of H_2 and H_2O, which results from the decomposition of carbonate minerals and the polycondensation reaction. The pore structure and heterogeneity of different rank coals treated at 200 °C remain stable except for the enlargement of the pore size because of the slight thermal expansion of the coal matrix and the removal of moistures/partial volatiles. However, as the temperature rises to 400 °C, the partial adsorption pores of low-rank coal (LRC) are closed, while the adsorption pore volume of medium-rank coal (MRC) increases, which may relate to the continuous decomposition of the volatile matter and the outburst of small-molecule gas. The massive seepage pores and microfractures are extensively developed in LRC (90.6% vol) and MRC (61.26% vol) treated at 600 °C, which provide an important flow pathway for coalbed methane recovery. In comparison, the pore structure and heterogeneity of high-rank coal (HRC) change indistinctly at 400 and 600 °C because of the original high metamorphic degree. Moreover, the pore compressibility values show a descending trend as the coal rank increases, corresponding to 2.45×10^{-4} to 3.09×10^{-2} MPa^{-1} for LRC, 9.43×10^{-4} to 4.03×10^{-2} MPa^{-1} for MRC, and 2.76×10^{-4} to 6.9×10^{-4} MPa^{-1} for HRC when the pressure and temperature range from 14.5 to 206 MPa and 25 to 600 °C, respectively. Meanwhile, the pore compressibility of coals shows a remarkable positive correlation with the pore volume fraction of micropores and transition pores, which can provide a large amount of compressible space at the high-pressure stage.

1. INTRODUCTION

As a clean and highly efficient hydrocarbon source, coalbed methane (CBM) has achieved extensive commercial development in the Unites States, Canada, and China in recent years.[1−4] Compared with conventional natural gas, CBM is mainly present in an absorbed form in the coal matrix,[5] and the production process of CBM involves the desorption of the gas from the pore surface by reducing the reservoir pressure and the subsequent promotion of gas migration from the matrix pore system to the cleat/fracture system.[6,7] In addition to the hydraulic fracturing and injection of CO_2 or other displacement gases, the in situ heat treatment of coals currently provides a feasible alternative for enhancing the CBM recovery.[8,9] Previous investigations have mostly focused on the structural behavior of coal at elevated temperature and the chemical aspect of coal pyrolysis/gasification,[10−12] while there is a limited amount of research on improving coal reservoir properties to facilitate CBM recovery after heat treatment.[13] Therefore, accurate characterization of the pore structure evolution at elevated temperatures and the thermomechanical response of coals are of great significance for enhancing the CBM flow capacity and maximizing the recovery.

Coal reservoirs are generally classified into two distinct groups: (1) the primary porosity system, which consists of a coal matrix with a high heterogeneity of micro- and mesopores, and (2) the secondary porosity system, which is composed of macropores and fractures/cleats.[14] According to Hodot[15] and Li et al.,[16] the pore network of coals can be divided by diameter into micropores (<10 nm), transition pores (10 to 10^2 nm), mesopores (10^2 to 10^3 nm), macropores (10^3 to 10^4 nm), and microfractures (>10^4 nm). Based on the heating experiments in muffle and thermal gravimetric analysis, Bustin and Guo[17] found that the chemical composition and reflectance values of coal experience multiple stages of abrupt changes as the temperature increases. Meanwhile, the development of pores at different scales in coal also changes significantly during these abrupt temperature changes or coalification jumps. By studying the

Received: January 12, 2020
Revised: February 21, 2020
Published: February 24, 2020

Table 1. Results of the $R_{o,m}$, Petrographic, and Proximate Analysis of the Selected Coal Samples[a]

			proximate analysis (%)				petrographic analysis (%)			
sample	sampling location	$R_{o,m}$ (%)	M_{ad}	A_{ad}	V_{ad}	FC_{ad}	V	I	L	M
LRC	EOB	0.58	2.95	13.87	32.44	50.74	68.43	21.84	7.38	2.35
MRC	EOB	1.65	0.52	13.56	12.15	73.77	77.00	21.8	0.0	1.20
HRC	SQB	3.12	1.83	8.43	9.36	80.38	75.06	19.14	0.0	5.80

[a]Note: EOB—Eastern Ordos Basin; SQB—Southern Qinshui Basin; M_{ad}—moisture content (wt %, air dry basis); A_{ad}—ash yield (wt %, air dry basis); V_{ad}—volatile matter (wt %, air dry basis); FC_{ad}—fixed carbon (wt %, air dry basis); V—vitrinite; I—inertinite; L—liptinite; and M—mineral.

changes of the coal pore surface structure with high-temperature treatment, Lorenz et al.[18] discovered that the micropore surface is formed at higher heating rates, and the larger micropore structure and pore surface area result from the higher initial particle heating rate. By investigating the pore fracture development of coals under high temperatures in a series of laboratory experiments, Yu et al.[19] and Yang et al.[20] found that the pore volume of coal experiences modest changes for temperatures ranging from 20 to 300 °C, large pores in coal greatly increase, the overall porosity reaches 23% at 400 °C, and the pore volume and porosity increase linearly for temperatures ranging from 400 to 600 °C. Meanwhile, the number and length of fractures increase, while the fracture rate and width first increase and then decrease as the temperature rises. Furthermore, based on our previous study,[21] the pore structure of low-rank coals (LRCs) remains nearly unchanged during low-heat treatment (25−200 °C), and the meso- and macropores are significantly developed for temperatures ranging from 400 to 600 °C. Overall, the production of organic decomposition products and the evolution of pore characteristics may also vary significantly according to various factors (such as the coal rank, maceral composition, heating rate, and retention time) during coal pyrolysis.

The volumetric change of coal reservoir due to pressure/stress variations is a critical factor affecting the CBM recovery and production simulation. Previous studies[22−26] have investigated the pore/matrix compressibility or cleat compressibility of coals using a series of laboratory measurements [such as mercury intrusion porosimetry (MIP) and confining pressure with the nuclear magnetic resonance method] and mathematical methods, which can more accurately calculate the coal permeability and predict the CBM production. Moreover, the mercury injection data for the high-pressure range (normally $P >$ 10 MPa) can also be corrected with compressibility coefficients by combining gas adsorption and MIP.[27,28] Although previous research has proposed that the temperature has critical implications for coal strength and stiffness,[29] there is still a lack of experimental and simulation results on the pore compressibility of coals under heat treatment. Furthermore, the response of the pore structure and compressibility for different rank coals with heat treatment has not yet been studied systematically. Thus, in this work, we first analyzed the thermal weight loss and organic decomposition products of different rank coals by thermogravimetry−mass spectrometry (TG−MS) during the heat treatment process (25−1200 °C). The characteristics of the generated gas (such as H_2, CH_4, H_2O, and CO_2) for different rank coals treated at different temperatures were analyzed. Second, the evolution characteristics of the pore networks and microfractures of heat-treated coals (25, 200, 400, and 600 °C) were investigated by combining N_2 adsorption and MIP methods. Meanwhile, a compressibility model based on fractal dimensions was proposed to calculate the pore compressibility of coals using the MIP data. Finally, the effects of coal rank and temperature on the pore compressibility of coals were analyzed, and the correlation between the pore structure and pore compressibility was discussed in detail.

2. SAMPLES AND METHODOLOGIES

2.1. Sampling and Coal Analyses. Three coal samples with a volume of ∼15 × 15 × 15 cm^3 were collected from the main coal reservoir of three active mines in the eastern Ordos Basin and southern Qinshui Basin of China. The maximum vitrinite reflectance ($R_{o,m}$) and the macerals and proximate analysis of coal samples were conducted using a Leitz MPV-3 photometer microscope and an Automatic Proximate Analyzer 5E-6600, respectively. As shown in Table 1, the results indicate that a low-rank coal (LRC) with a $R_{o,m}$ of 0.58% and a medium-rank coal (MRC) with a $R_{o,m}$ of 1.65% are originated from eastern Ordos Basin, and the coal sample collected from the southern Qinshui Basin belongs to the high-rank coal (HRC, 3.12% $R_{o,m}$).

2.2. Experimental Procedures. *2.2.1. TG−MS Analysis during Heat Treatment.* The TG−MS analysis was performed using a SETSYS Evolution TG−differential thermal analysis analyzer coupled with an OMNI star MS in the State Key Laboratory of Coal Conversion, Institute of Coal Chemistry, China. The coal sample in the programmed furnace was continuously heated from 25 to 1200 °C with a heating rate of 10 °C/min, a constant sweeping nitrogen rate of 60 cm^3/min, and a retention time of 30 min, as introduced in our previous research.[21] The coal sample weight was measured continuously during the heat treatment, which can be used to analyze the differential thermal gravity (DTG). Meanwhile, the gas generated in the TG analyzer could flow into the mass spectrometer through the connection line and was scanned with intervals of ∼19 s for the mass-to-charge ratio (m/z) of 1−100 amu. The information of organic decomposition products with elevated temperature was obtained by the multiple ion detection modes of MS.

2.2.2. N_2 Adsorption/Desorption and MIP Measurements. The N_2 adsorption/desorption experiment was conducted on the Micromeritics ASAP-2000 automated analyzer at 77 K in the Coal Reservoir Laboratory of National Engineering Research Center of CBM Development & Utilization, China. Before the test, different rank coal samples were heat treated by 25, 200, 400, and 600 °C in a tube furnace under the flow of nitrogen gas. Then, the heat-treated coal samples were crushed and sieved to 60−80 mesh (0.18−0.25 mm) particles and dried at 110 °C for 24 h in a vacuum oven to remove free water and other impurity substances.[30] During the experimental process, the N_2 adsorption and desorption data were obtained under the relative pressure (P/P_0) range of 0.01−0.995. Based on the adsorption data, the pore structure parameters (such as specific surface area, pore volume, and pore size distribution) were calculated by the

https://dx.doi.org/10.1021/acs.energyfuels.0c00135
Energy Fuels 2020, 34, 3173−3187

Table 2. Pore Structure Parameters and Fractal Dimensions Derived from N_2 Adsorption/Desorption Analysis of Coal Samples at Elevated Temperatures[a]

					P/P_0: 0−0.9		P/P_0: 0.9−1.0		
sample	T (°C)	BET-specific surface area (m^2/g)	BJH volume (10^{-3} cm^3/g)	average pore diameter (nm)	A_1	$D_{N1} = 3 + A_1$	A_2	$D_{N2} = 3 + A_2$	hysteresis loop types
LRC	25	0.773	3.729	27.49	−0.41	2.59	−0.37	2.63	H1
	200	0.301	1.777	35.09	−0.28	2.72	−0.46	2.54	H1
	400	0.066	0.74	48.86	−0.25	2.75	−0.64	2.36	H2
	600	0.951	1.281	84.35			−0.68	2.32	H5
MRC	25	0.88	4.858	52.07	−0.14	2.86	−0.67	2.33	H4
	200	0.84	5.503	52.36	−0.15	2.85	−0.69	2.31	H4
	400	0.667	6.554	63.77	−0.30	2.70	−0.80	2.20	H4
	600	0.775	3.826	81.87			−1.46	1.54	H5
HRC	25	1.549	2.062	18.81	−0.07	2.93	−0.31	2.69	H4
	200	0.973	1.941	19.35	−0.08	2.92	−0.37	2.63	H4
	400	0.83	1.451	22.73	−0.09	2.91	−0.32	2.68	H4
	600	1.707	2.323	47.57	−0.06	2.94	−0.27	2.73	H5

[a]Note: D_{N1}—fractal dimension of micropores with P/P_0 ranging from 0 to 0.9 and D_{N2}—fractal dimension of transition pores with P/P_0 ranging from 0.9 to 1.0.

Table 3. Pore Structure Characteristics and Fractal Dimensions of Coal Samples at Elevated Temperatures Analyzed by MIP[a]

							pore volume distribution (%)					
sample	T (°C)	V_m (cm^3/g)	MIS (%)	EMW (%)	MPT (μm)	sorted coefficient	<10^2 nm	10^2 to 10^3 nm	>10^3 nm	D_{M1}	D_{M2}	curve type
LRC	25	4.03×10^{-2}	66.98	79.48	0.113	0.477	81.37	11.03	7.60	2.96	3.86	I
	200	4.32×10^{-2}	64.03	79.20	0.097	0.366	81.43	9.89	8.68	2.92	3.93	I
	400	5.26×10^{-2}	62.28	62.50	0.195	0.523	64.46	16.55	18.99	2.86	3.63	II
	600	0.241	77.49	6.450	0.639	0.654	9.40	32.55	58.05	2.49	3.34	IV
MRC	25	4.96×10^{-2}	79.66	62.74	0.092	0.264	52.32	44.00	3.68	2.87	3.14	III
	200	5.26×10^{-2}	82.05	53.05	0.21	0.454	47.09	38.04	14.87	2.82	3.17	III
	400	6.04×10^{-2}	76.72	69.45	0.088	0.269	67.81	26.27	5.92	2.8	3.21	III
	600	5.31×10^{-2}	97.88	64.63	0.276	0.496	38.74	45.73	15.53	2.68	3.08	III
HRC	25	0.347	77.95	6.94	74.86	51.47	6.79	0.52	92.68	2.55	3.93	V
	200	0.222	82.18	10.11	89.77	45.72	9.81	0.98	89.21	2.52	3.93	V
	400	0.363	72.82	6.57	91.20	48.90	6.52	0.96	92.52	2.49	3.81	V
	600	0.385	75.90	5.91	69.38	51.17	5.87	0.62	93.51	2.29	3.86	V

[a]Note: V_m—total mercury intrusion volume; MIS—mercury injection saturation; EMW—efficiency of mercury withdrawal; MPT—mean pore throat radius; D_{M1}—fractal dimension with P < 14.5 MPa; and D_{M2}—fractal dimension with P > 14.5 MPa.

Brunauer−Emmett−Teller (BET) and Barrett−Joyner−Halenda (BJH) methods (Table 2).

The MIP measurement was performed with a PoreMasterGT60 Instrument, which automatically registers the mercury intrusion/extrusion pressure and corresponding volume. The heat-treated coal sample was selected for MIP measurements and the instrument could reach a maximum pressure of 206 MPa, corresponding to the smallest pore size of 7.0 nm.[21] The total mercury intrusion volume (V_m), mercury injection saturation (MIS), and efficiency of mercury withdrawal (EMW) were measured and are presented in Table 3. Moreover, the pore radius can be calculated by the Washburn equation[31]

$$P_c = -\frac{2\delta \cos\theta}{r_c} = \frac{0.735}{r_c} \quad (1)$$

where P_c is the mercury injection pressure, MPa; r_c is the pore radius, μm; θ is the contact angle, 140°; and δ is the interfacial tension of mercury, 0.48 J/m^2. On this basis, the pore volume and pore size distribution can also be inferred from the mercury intrusion data.

2.3. Fractal Theory of N_2 Adsorption and MIP Measurements. The fractal theory is very convenient to characterize the irregular structure of porous media and provides a quantitative analysis method to describe the complexity of porous media with no characteristic length scale. Based on the N_2 adsorption data, the Frenkel−Halsey−Hill (FHH) model has been certified as the most effective and frequently used method to calculate the fractal dimension of adsorption pores (diameter <100 nm) in coals.[32] According to the FHH model, the relationship between the volume of adsorbed gas (V) and the equilibrium pressure (P) can be described as follows

$$\ln V = A\left[\ln\left(\ln \frac{P_0}{P}\right)\right] + C \quad (2)$$

where P_0 is the saturation pressure of adsorbed gas; C is a constant; and A is the slope of linear fitting between ln V and ln(ln(P_0/P)). The fractal dimension (D_N) of adsorption pores is generally calculated by two different formulas, namely, "$D_N = A + 3$" and "$D_N = 3A + 3$".[30,32] However, the values of D_N obtained from "$D_N = 3A + 3$" are usually lower than 2.0 and deviate from the normal fractal dimension value (2.0−3.0) of pore structure. Therefore, the fractal dimension of adsorption pores should be calculated using "$D_N = A + 3$" (Table 2).

Based on the mercury intrusion data and the Washburn equation, Friesen and Mikula[33] discovered that the cumulative mercury intrusion volume (V) and mercury intrusion pressure

https://dx.doi.org/10.1021/acs.energyfuels.0c00135
Energy Fuels 2020, 34, 3173−3187

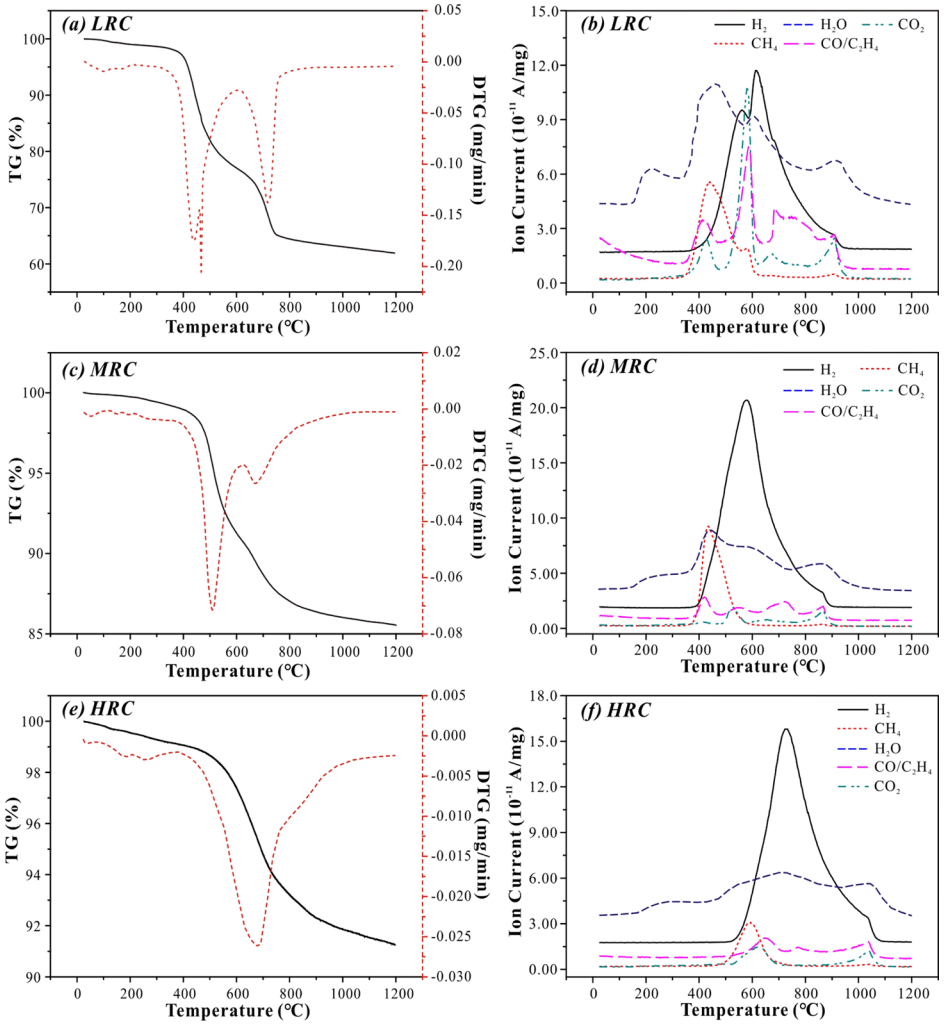

Figure 1. Thermal weight loss and gas generation characteristics of different rank coals during the heat treatment between 25 and 1200 °C with a heating rate of 10 °C/min.

(P) show a double-logarithmic fitting relationship, as shown below

$$\log\left(\frac{dV}{dP}\right) \propto (D_M - 4)\log(P) \quad (3)$$

where D_M is the fractal dimension of the pore structure from the MIP data, which can be obtained by the slope of eq 3. Moreover, the calculated fractal dimension of the adsorption pores exceeds 3.0 because the compression effect of the coal matrix is nontrivial and cannot be negligible in a high-pressure range (approximately > 13 MPa),[34] which was used to study the pore compressibility in this study.

3. RESULTS AND DISCUSSION

3.1. Thermogravimetric and Gas Generation Characteristics. The thermal weight loss and gas generation characteristics of different rank coals during the heat treatment process (25−1200 °C) are shown in Figure 1. The total thermal weight loss of the LRC sample (~40%) is much greater than that of the MRC sample (~15%) and HRC sample (~9%) (Figure 1a,c,e), which is mainly controlled by the volatile content of different rank coals (Table 1). For the LRC and MRC samples, the heat treatment process can be divided into four stages: (1) the first stage generally occurs at a temperature below 350 °C, in which the moisture and a small amount of other gases (such as CH_4 and CO_2) that are adsorbed in the coal matrix are gradually removed as the temperature increases (Figure 1b,d), which results in the weight loss of coals (~1.0−2.5%) in this stage not being obvious; (2) the second stage mainly takes place at 350−600 °C and is accompanied by the maximum weight loss of coals (~5.0−12.5%) with a peak at ~450−500 °C, in which the macromolecular organic matter is decomposed into coal tar and small molecular gas products, including a large amount of H_2, H_2O, CH_4, C_2H_4/CO, CO_2, and other gases (Figure 1b,d); (3) the continuous thermal weight loss appears in the third stage (600−950 °C), and meanwhile, the production peak of CO and CO_2 is approximately 700−800 °C and coincides with the presence of H_2 and H_2O, which probably results from the decomposition of carbonate minerals and the polycondensation/dehydrogenation reaction of aromatic lamellar and secondary reactions (such as $H_2O + C \rightleftharpoons H_2 + CO$ and $2CO \rightleftharpoons CO_2 + C$);[35] (4) the final stage generally occurs at temperatures higher than 950 °C, in which the weight of coals tends to be stable as the temperature increases, and small amounts of molecular gas are basically not generated (Figure 1b,d). However, according to the TG−DTG curve of the HRC sample, the process of thermal weight loss only consists of three stages (Figure 1e): the first and final stages are the same as those

https://dx.doi.org/10.1021/acs.energyfuels.0c00135
Energy Fuels 2020, 34, 3173−3187

of the other two samples, whereas the middle stage of the HRC sample shows a continuous thermal weight loss with temperatures ranging from 350 to 950 °C and the fastest weight loss appears at $T_{DTG_{max}}$ = 700 °C. In the middle stage, the HRC sample only generates a small amount of hydrocarbon gases (such as CH_4 and C_2H_4) and water at 350−600 °C, and then the production peaks of CO_2, H_2, and H_2O coexist at 600−800 °C (Figure 1f), suggesting that gas generation by the HRC sample may be mainly controlled by the decomposition of carbonate minerals and the polycondensation reaction during heat treatment, which is consistent with the research of Solomon et al.[36] CH_4 is mainly generated at temperatures between 350 and 600 °C and reaches a peak at ∼450 °C for low- and medium-metamorphic coals, whereas the CH_4 generated from high-metamorphic coal is found at temperatures between 500 and 700 °C. This phenomenon may be related to the breakdown of long-chained aromatic groups with -alkyl/-ether bonds and the secondary cracking of long-chain hydrocarbons in coals.[35,37] Therefore, suitable temperatures for increasing methane content in coal reservoirs and enhancing CBM recovery should not exceed 700 °C, which may also improve the petrophysics of the coal reservoir.

3.2. Evolution of the Pore Structure during Heat Treatment. *3.2.1. Pore Morphology by SEM Observations.* Figure 2 shows the pore and surface morphology evolution of the LRC and MRC samples undergoing heat treatment at different temperatures, respectively. The isolated primary pores are developed in the unheated LRC sample (Figure 2A), and the matrix surface morphology of the MRC sample is relatively smooth (Figure 2a). After heat treatment at 200 °C, the surface morphology of the LRC sample basically retains its original appearance, and partial pores are enlarged or closed (Figure 2B), which may be related to the removal of volatiles/moistures and slight thermal expansion at a temperature of 200 °C.[19,21] As shown in Figure 2b, the surface morphology of the MRC sample treated at 350 °C begins to soften, and the macropore structure has changed only slightly in contrast with the unheated MRC sample. When the temperature reaches 400 °C, the surface morphology of the LRC sample exhibits the squamous structure and the pore morphology tends to be wedge-shaped or elliptical with a significantly increased diameter (Figure 2C). Moreover, as shown in Figure 2c, plastic deformation is evident in the MRC sample at 450 °C, and the proportion of macropores increases obviously.[38] On the one hand, the softening and thermal shrinkage of the coal matrix contribute to the plastic deformation or squamous structure of the coal surface morphology. On the other hand, the decomposition of macromolecular organic matter and gas outbursts lead to the increase of the pore diameter and the proportion of macropores in coals at 400−450 °C. As the temperature rises to 600 °C, the surface morphology changes to a spongy/honeycomb-shaped structure, and massive macropores are generated in the LRC and MRC samples (Figure 2D,d), suggesting that a large amount of gases are generated, and outburst may further enlarge the original pores and create a large number of macropores. Therefore, the heat treatment will improve the physical properties of coals and then enhance the CBM flow capacity and recovery.

3.2.2. Adsorption Pore Structure by N_2 Adsorption/Desorption. Figure 3 demonstrates the variation of the BET pore surface area, BJH pore volume, and average pore diameter of coal samples at elevated temperatures. An interesting

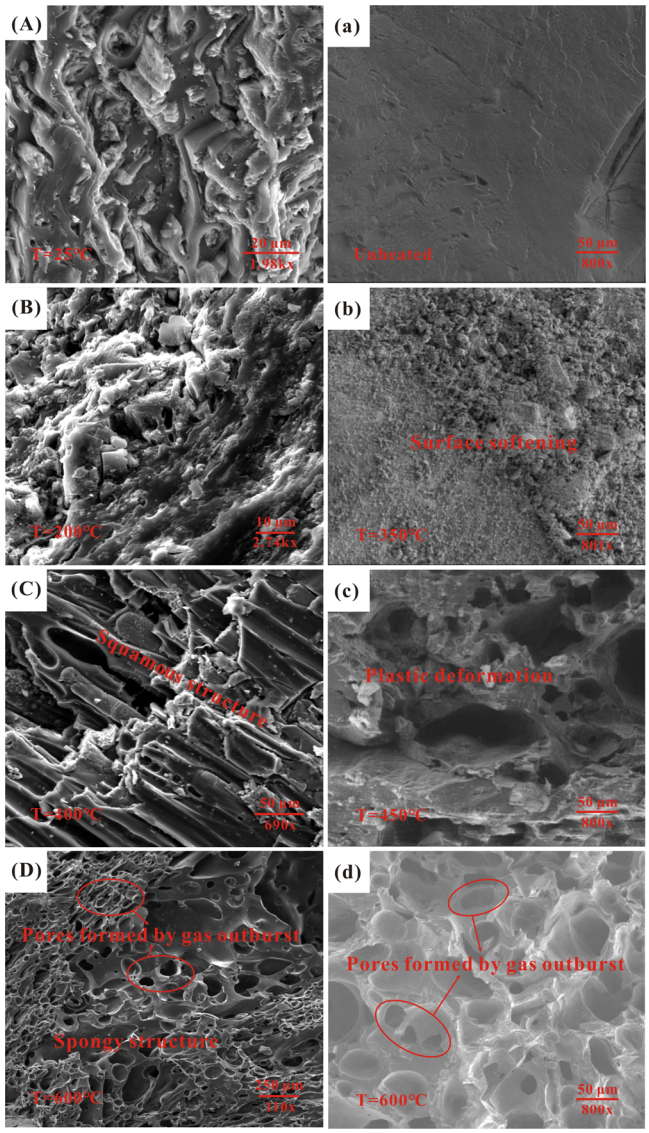

Figure 2. Pore and surface morphology evolution of coal samples undergoing heat treatment at different temperatures (modified from Li et al.[21] and Gneshin et al.,[38] Copyright 2015, American Chemical Society): (A) LRC sample, 25 °C; (B) LRC sample, 200 °C; (C) LRC sample, 400 °C; (D) LRC sample, 600 °C; (a) MRC sample, unheated; (b) MRC sample, 350 °C; (c) MRC sample, 450 °C; and (d) MRC sample, 600 °C.

phenomenon is that the pore surface area of different rank coal samples first decreases when the temperature rises from 25 to 400 °C and then increases as the temperature continuously rises to 600 °C (Figure 3a). This may be related to the thermal softening phenomenon of the coal matrix before 400 °C, resulting in the closure of partial adsorption pores and a reduction of the pore surface area. Then, because of the continuous decomposition of volatile matter and the outburst of small-molecule gas, the quantity of adsorption pores increases significantly between 400 and 600 °C,[39] which causes a marked increase in the pore surface area. The pore volume variation of the LRC and HRC samples at elevated temperatures coincides with the change of the pore surface area, whereas that of the MRC sample first increases as the temperature increases from 25 to 400 °C and then decreases at temperatures ranging from 400 to 600 °C (Figure 3b). This indicates that the development of

https://dx.doi.org/10.1021/acs.energyfuels.0c00135
Energy Fuels 2020, 34, 3173−3187

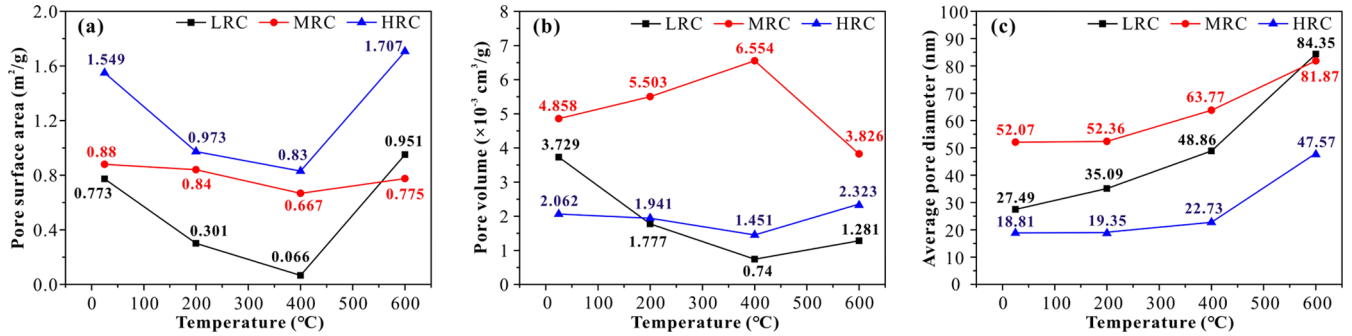

Figure 3. Variation of BET pore surface area, BJH pore volume, and average pore diameter of different rank coal samples treated at different temperatures.

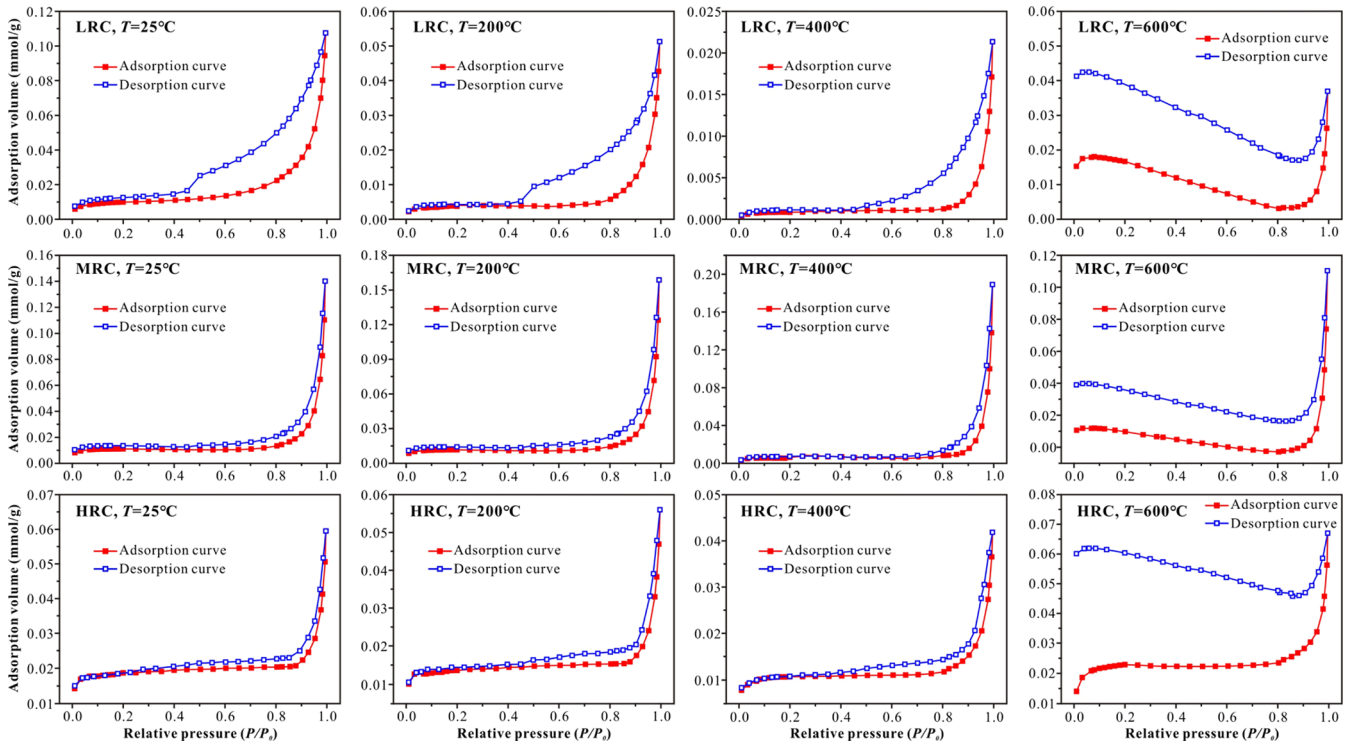

Figure 4. N_2 adsorption/desorption isotherms of different rank coal samples at elevated temperatures.

adsorption pores at different scales at elevated temperatures and the contribution of elevated temperatures to the pore volume may control the pore volume variation characteristics of different rank coals. Moreover, the average pore diameter of different coal samples is gradually enlarged as the temperature rises from 25 to 600 °C (Figure 3c).

According to the classification proposed by Yao and Liu,[40] the N_2 adsorption/desorption isotherms of coal samples with elevated temperatures demonstrated three typical types (H1, H2, and H4) and an abnormal type (H5) in this study, as depicted in Figure 4. The isotherms of the LRC sample at temperatures of 25 and 200 °C belong to type H1, for which a distinct hysteresis loop exists at a P/P_0 of 0.45−1.0 and a sharp inflection point appears at a P/P_0 of ∼0.5. In contrast, the isotherm of the LRC sample treated at 400 °C is type H2, which has an obvious hysteresis loop but no inflection point at a P/P_0 of ∼0.5. When the temperature reaches 600 °C, the isotherm of the LRC sample demonstrates the abnormal type H5, for which the absorption/desorption capacity decreases as the pressure increases and the adsorption and desorption curves cannot be closed. This indicates that the adsorption pore morphology of the LRC sample is mainly ink-bottle pores/fine bottleneck pores at 25−200 °C and then changes to open cylinder pores or parallel plate pores at 400 °C. Because of the increased proportion of fixed carbon and the well-developed super micropores (<1.0 nm) in the LRC sample at 600 °C, it is difficult or impossible for nitrogen gas molecules to enter super micropores, and their adsorption property becomes very complicated, which may result in an abnormal adsorption/desorption behavior. Moreover, the pore surface area and pore volume of the LRC sample are dominated by micropores and transition pores with diameter ranging from 5 to 80 nm at 25 and 200 °C, whereas those of the LRC sample at 400 and 600 °C are mainly controlled by transition pores with diameter ranging from 10 to 80 nm (Figure 5a,b). The adsorption pore structure evolution of the LRC sample during heat treatment is conducive to CBM desorption and diffusion.

For the MRC and HRC samples, the adsorption/desorption isotherms for temperatures of 25, 200, and 400 °C all belong to type H4, which shows a narrow hysteresis loop at a P/P_0 of

https://dx.doi.org/10.1021/acs.energyfuels.0c00135
Energy Fuels 2020, 34, 3173−3187

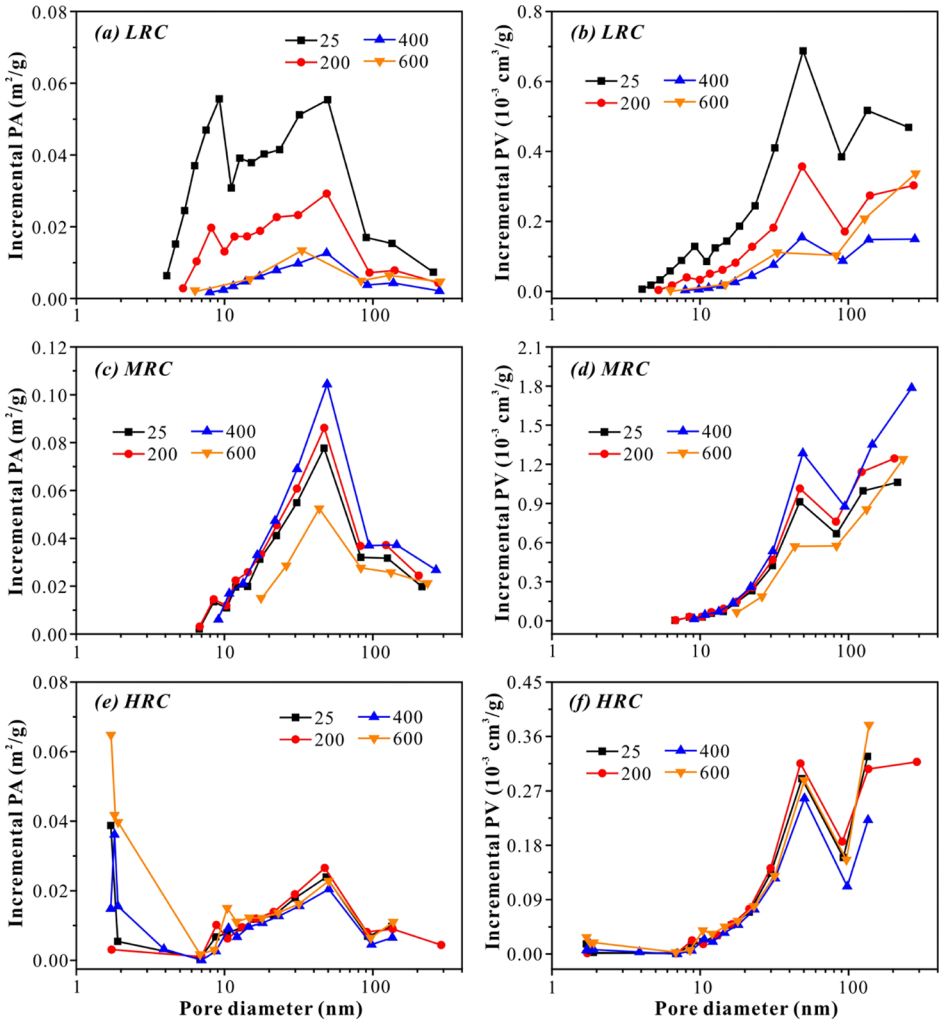

Figure 5. Pore surface area and pore volume distribution of different rank coal samples by N_2 adsorption analysis.

0.45−1.0 and is evidenced by the slit- or wedge-shaped pores with one open side. By comparison, the isotherms of the MRC and HRC samples treated at 600 °C exhibit the abnormal type H5, which is the same as the LRC sample. Furthermore, the transition pores with diameters ranging from 20 to 80 nm mainly contribute to the pore surface area and pore volume of the MRC sample during the heat treatment (Figure 5c,d), indicating that this pore structure is beneficial to the desorption and diffusion of CBM. However, the pore surface area of the HRC sample is dominated by micropores (2.0−8.0 nm) and transition pores, and the pore volume is also mainly controlled by transition pores (Figure 5e,f), which is conducive to the adsorption and storage capacity of CBM. Therefore, the process of heat treatment does not change the morphology and pore size distribution of adsorption pores but only changes the pore surface area and total pore volume of medium- and high-metamorphic coals.

3.2.3. Seepage Pore Structure by MIP Analysis. Because of the increased compressibility of the coal matrix in the high-pressure range, the MIP method is commonly used to characterize the seepage pores (diameter >100 nm).[21,28] As shown in Table 3, the V_m of the LRC sample significantly increases from 4.03×10^{-2} to 0.241 cm^3/g as the temperature increases from 25 to 600 °C; meanwhile, the EMW sharply decreases from ∼80 to 6.45%. However, there is no obvious variation in the V_m and EMW of the MRC (4.96×10^{-2} to 6.04×10^{-2} cm^3/g and 53.05−69.45%) and HRC (0.222−0.385 cm^3/g and 5.91−10.11%) samples at elevated temperatures. This phenomenon suggests that although the process of heat treatment can effectively promote the development of meso-/macropores in the LRC sample, the connectivity of pores and fractures can also be reduced with high-temperature treatment (400−600 °C) as a result of the coal tar condensing and blocking the pore throats. Moreover, the seepage pores/microfractures and the connectivity of the medium- and high-metamorphic coals (MRC and HRC) show no obvious improvement during the heat treatment.

Based on the comprehensive analysis of various classification methods,[40,41] the mercury intrusion curves of coal samples with elevated temperatures can be divided into five types (I, II, III, IV, and V) in this study (Table 3). The typical characteristics of the five curves and the pore size distribution of coal samples at different temperatures are shown in Figure 6. The mercury intrusion curves of the LRC sample belong to type I for temperatures of 25 and 200 °C, to type II for a temperature of 400 °C, and to type IV for a temperature of 600 °C (Figure 6a). The mercury intrusion curves for all these samples present three distinct segments, and the mercury volumes of all the samples hardly increase when $P < 0.2$ MPa. However, for the type I curve, the mercury volume increases slowly (∼1/3 vol) in the pressure range of 0.2−20 MPa and then increases quickly (∼2/3 vol)

https://dx.doi.org/10.1021/acs.energyfuels.0c00135
Energy Fuels 2020, 34, 3173−3187

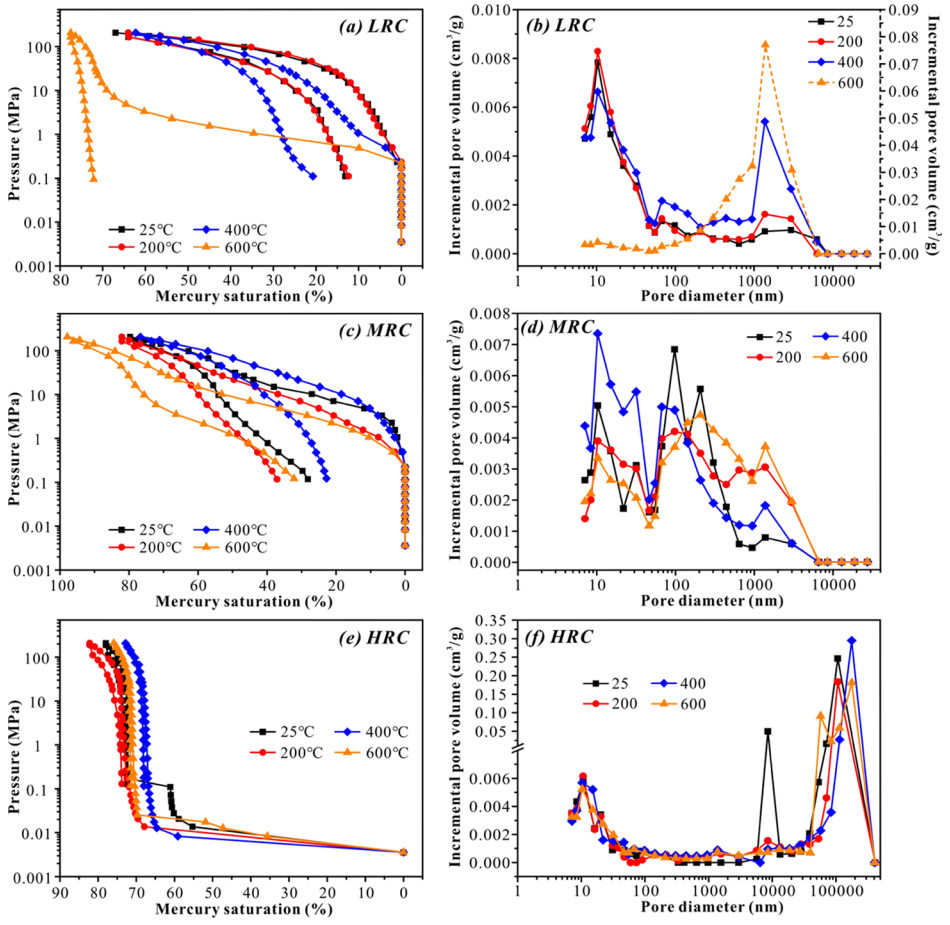

Figure 6. Mercury intrusion/extrusion curves and corresponding pore size distribution of different rank coal samples at elevated temperatures.

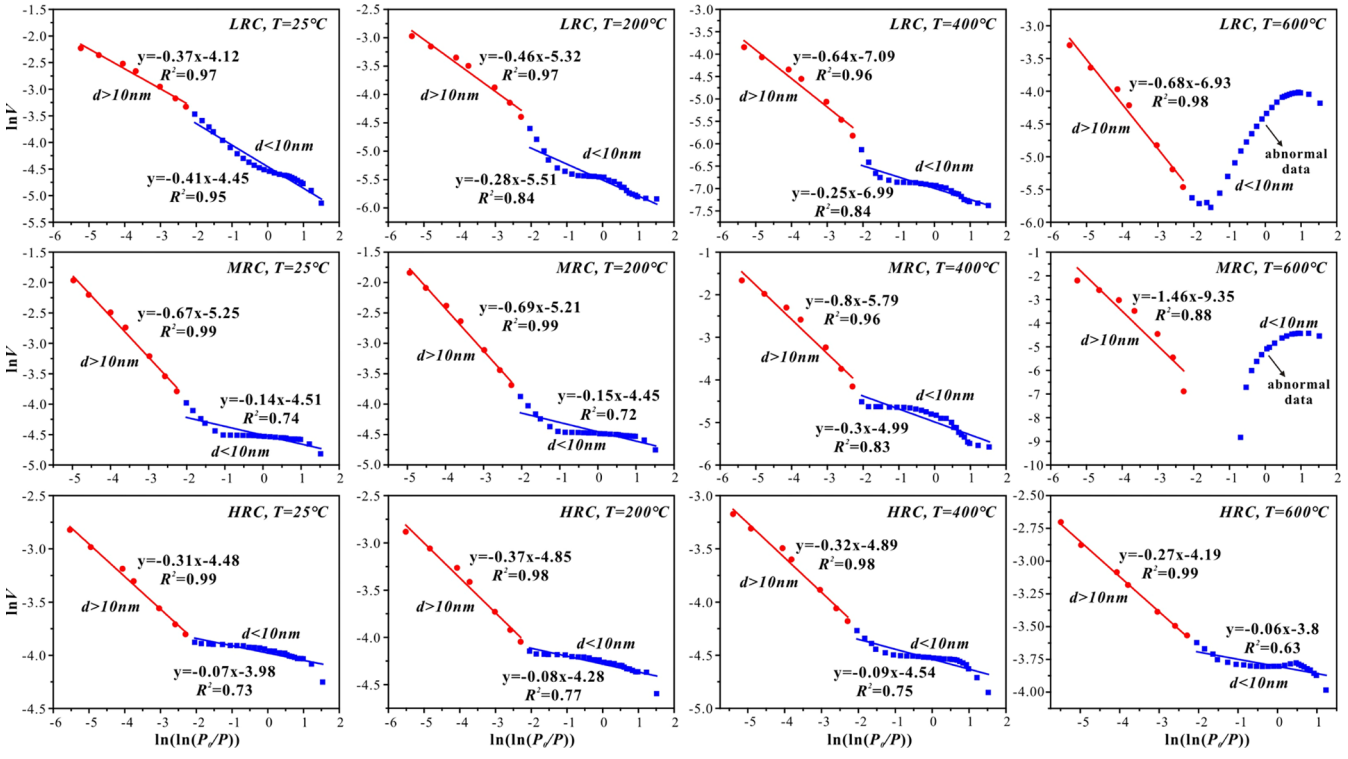

Figure 7. Plots of ln V vs $\ln(\ln(P_0/P))$ of different rank coal samples reconstructed from the N_2 adsorption data.

https://dx.doi.org/10.1021/acs.energyfuels.0c00135
Energy Fuels 2020, 34, 3173−3187

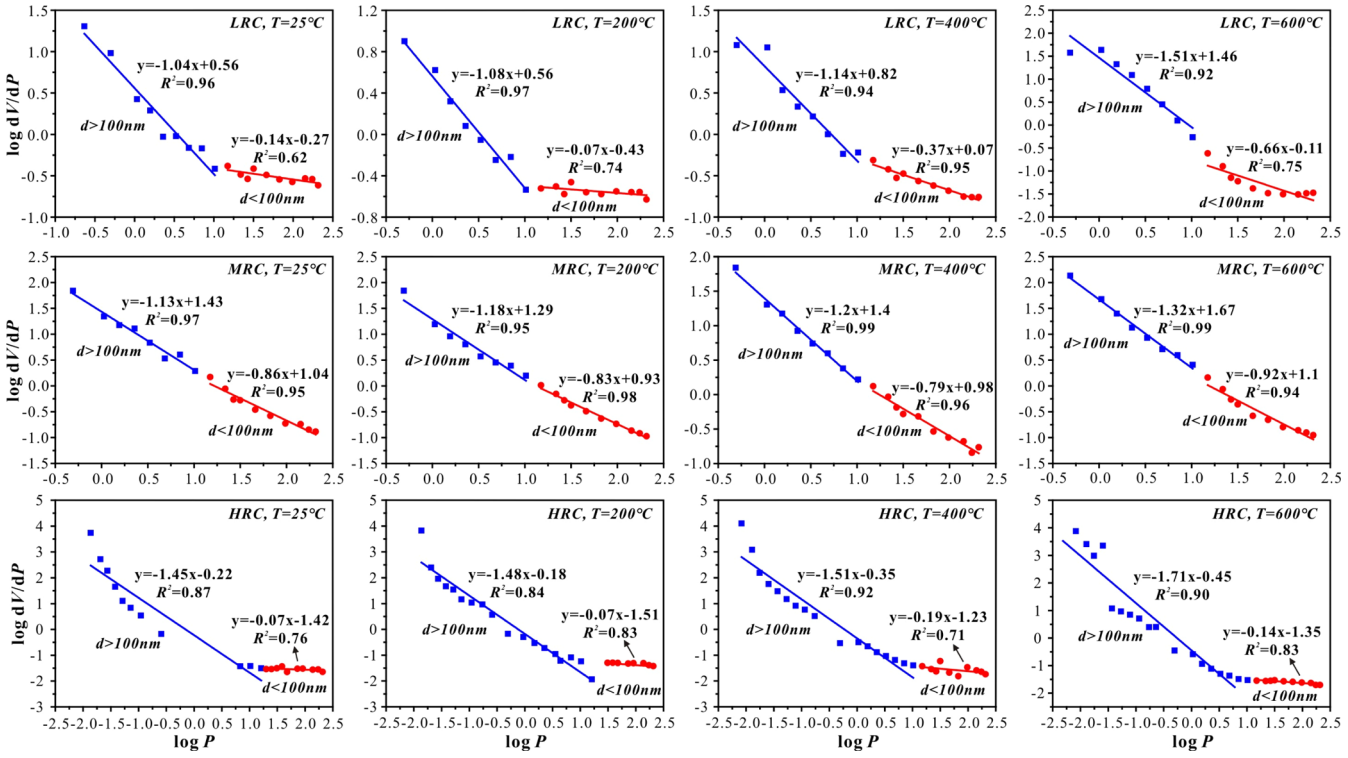

Figure 8. Plots of ln(dV/dP) vs ln P of different rank coal samples reconstructed from the MIP data.

when P > 20 MPa. The mercury volume accounts for ∼50% of the total volume in the range of 0.2−20 MPa and P > 20 MPa for the type II curve, whereas mercury is rapidly injected into the coal within 0.2−10 MPa (∼90% vol) for the type IV curve and hence the accumulated mercury volume is extremely tiny (∼10% vol) when P > 10 MPa. This indicates that the LRC sample treated at 25 and 200 °C mainly develops adsorption pores with proportion higher than 80%, and yet the mesopores and macropores increase to 16.55 and 18.99% when the temperature increases to 400 °C, respectively (Figure 6b). Furthermore, the LRC sample treated at 600 °C mainly consists of well-developed macropores (58.05%), moderately developed mesopores (32.55%), and a few adsorption pores (9.40%). The high-temperature heat treatment (400−600 °C) can generate a large amount of seepage pores in low-metamorphic coal, which provides an important flow pathway for CBM recovery. Comparatively, the mercury intrusion curves of the MRC sample at 25, 200, 400, and 600 °C always exhibit type III curves, in which the mercury volume also hardly increases when P < 0.2 MPa and then increases steadily when P > 0.2 MPa (Figure 6c). This phenomenon is related to the pore networks with a multimodal distribution of the MRC sample at elevated temperatures (Figure 6d). The seepage pores of the MRC sample treated at 200 and 600 °C are improved to 52.91 and 61.26% because of the removal of moistures/volatiles and gas outbursts under the decomposition of organic matter,[13] whereas the proportion of seepage pores decreases to 32.19% because of the thermal shrinkage of the coal matrix at 400 °C. As shown in Figure 6e, the mercury intrusion curves of the HRC sample at 25, 200, 400, and 600 °C all present type V curves with two distinct segments: (1) the mercury intrusion curve becomes horizontal, and the mercury volume increases rapidly (∼80% vol.) when P < 0.02 MPa; and (2) the mercury intrusion curve is approximately vertical, and the accumulated mercury volume is comparatively tiny (∼20% vol) when P > 0.02 MPa. A large amount of seepage pores (89.21−93.51%) developed in the HRC sample at different temperatures and mainly consist of well-developed microfractures and a few meso- and macropores (Figure 6f). Overall, the seepage pore structure of high-metamorphic coals does not change significantly during heat treatment.

3.3. Fractal Characteristics and Pore Heterogeneity Variation. The Kelvin equation is generally used to calculate the pore diameter of coals by N_2 adsorption data, and the pore diameter reaches 10 nm when P/P_0 is equal to 0.9.[27] Accordingly, the fractal dimensions of micropores (P/P_0 < 0.9) and transition pores (P/P_0 > 0.9) recognized from the linear fitting between ln V and ln(ln(P_0/P)) by the FHH model are shown in Figure 7. The fitting results show that the transition pores of different rank coal samples under heat treatment presents remarkable fractal characteristics (R^2 > 0.95 except for the MRC sample at 600 °C), whereas the fractal characteristics of micropores become relatively weak (R^2 < 0.85 in most cases) during high-temperature treatment and abnormal data even appears in the LRC and MRC samples at 600 °C. As can be seen in Table 2, the fractal dimension of the micropores (D_{N1}) for the LRC sample increases from 2.59 to 2.75 as the temperature increases (25−400 °C), whereas that of the transition pores (D_{N2}) shows a descending trend from 2.63 to 2.32 as the temperature increases (25−600 °C). This indicates that the removal of moistures and partial volatiles reduces the surface heterogeneity of transition pores during the low-temperature stage (25−200 °C), while the thermal shrinkage of the coal matrix makes the surface and structure of micropores (mainly ink-bottle pores) more complicated in this stage. As the coal matrix softens and a large amount of gas outburst pores are generated (400−600 °C), transition pores are dominated by regular cylinder pores or parallel plate pores, which results in a decrease in the heterogeneity of the pore surface and structure. Moreover, both the D_{N1} and D_{N2} of the MRC sample slightly

https://dx.doi.org/10.1021/acs.energyfuels.0c00135
Energy Fuels 2020, 34, 3173−3187

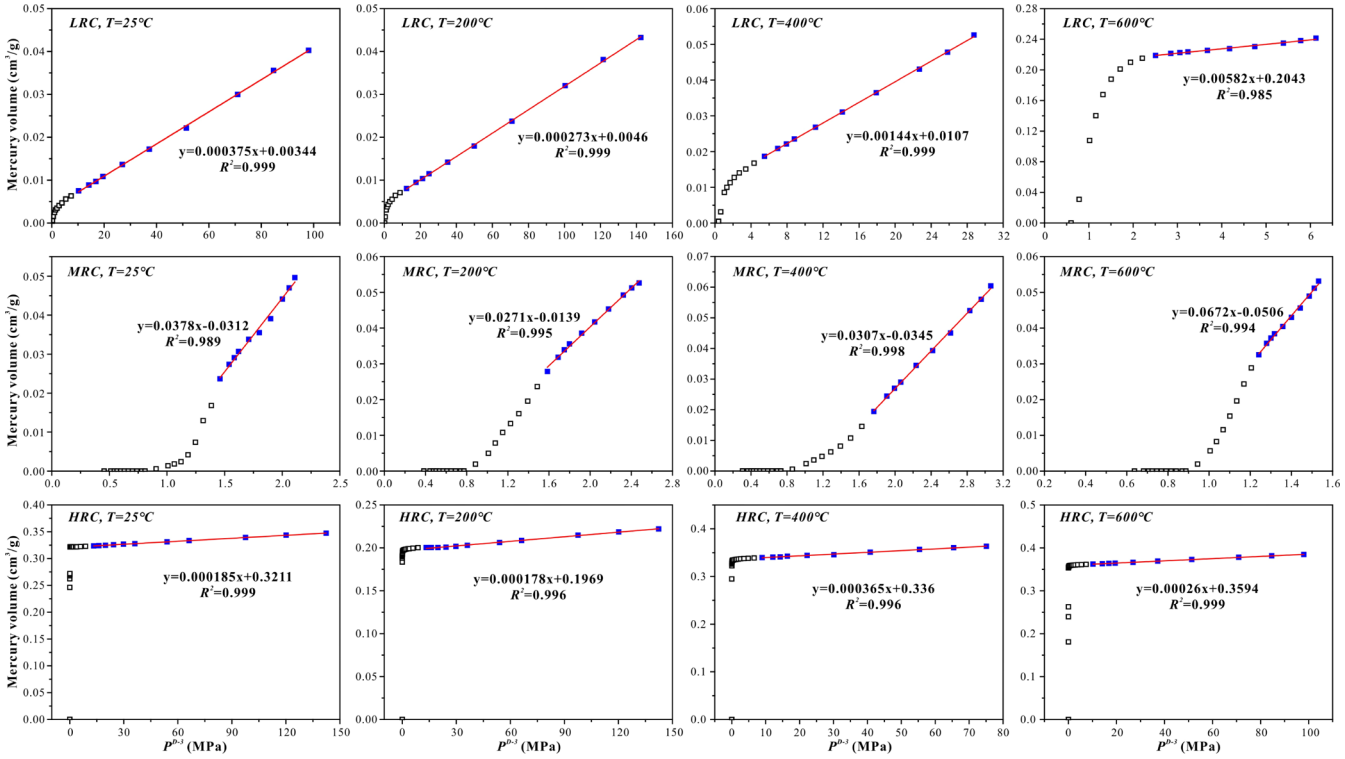

Figure 9. Relationship between the mercury intrusion volume and P^{D-3} of different rank coal samples at elevated temperatures.

decrease from 2.86 to 2.70 and 2.33 to 2.20 as the temperature increases (25−400 °C), respectively. This phenomenon may be related to the stable pore morphology and decreasing pore-specific surface area of the MRC sample during the heat treatment. In addition, the D_{N1} and D_{N2} of the HRC sample show no obvious change as the temperature increases (25−600 °C), corresponding to values of 2.91−2.94 and 2.63−2.73, respectively (Table 2). Thus, heat treatment at temperatures lower than 600 °C might not change the adsorption pore heterogeneity of the HRC sample because of its original high metamorphic degree.

Based on eq 3, Figure 8 shows the double logarithmic fitting plots between log(dV/dP) and log P of the mercury intrusion data. The MIP fractal dimension of the seepage pores (D_{M1}) for different rank coal samples shows a descending trend as the temperature increases (25−600 °C), with ranges from 2.96 to 2.49 for the LRC sample, 2.87−2.68 for the MRC sample, and 2.55−2.29 for the HRC sample (Table 3). As shown in the scanning electron microscopy (SEM) images (Figure 2), the heat treatment is liable to lead to a more regularized seepage pore morphology and smoother pore surface, which further reduces the surface heterogeneity of seepage pores. Moreover, the MIP fractal dimension of the adsorption pores (D_{M2}) for coal samples has totally exceeded 3.0 when the pressure >14.5 MPa (Figure 8 and Table 3). This phenomenon shows that the compression of the microporous structure and the coal particles gradually affects the pore-filling process. Meanwhile, the dV_p/dP ratio in eq 3 would approach constant and be completely independent of pressure as D_{M2} gradually approaches 4.0, which indicates that the pore-filling process has terminated and the increase of the mercury intrusion volume is entirely caused by the compression of pores and coal particles.[23,42] Through a fractal dimension analysis of the high-pressure stage during mercury intrusion, the pore compressibility of coals and its effect on the pore-filling process can be revealed.

3.4. Estimation of Pore Compressibility from MIP Analysis. The pore compressibility of coal (C_p, MPa^{-1}) is defined as the influence of pressure variations on the volume of pore space and represents the volume of excess fluid that can be stored in or flow through the pore space, which can be expressed as follows[43]

$$C_p = \frac{1}{V_p}\left(\frac{dV_p}{dP}\right) \tag{4}$$

where V_p is the pore volume of coals (cm^3/g) and dV_p/dP denotes the pore volume change of coal as a function of pressure. On this basis, eq 4 could be written as

$$d \ln V_p = C_p \, dP \tag{5}$$

$$\int_{\ln V_{P_1}}^{\ln V_{P_2}} d \ln V_p = \int_{P_1}^{P_2} C_p dP \tag{6}$$

The pore compressibility of coal is related to pressure and can be regarded as a constant when the pressure range ($\Delta P = P_{i+1} - P_i$) is small enough. Therefore, eq 6 can be simplified as follows

$$\ln \frac{V_{P_{i+1}}}{V_{P_i}} = C_{p_i}(P_{i+1} - P_i) \tag{7}$$

In combination with the fractal dimension at the high-pressure stage, the relationship between V_p and P can be converted to

$$V_p = a + bP^{D-3} \tag{8}$$

where a and b are constants. Because of the uncertain relationship between V_p and the mercury intrusion volume

https://dx.doi.org/10.1021/acs.energyfuels.0c00135
Energy Fuels 2020, 34, 3173−3187

Table 4. Constants *a* and *b* Obtained from MIP Data and the Calculation Formulas of Pore Compressibility for Coal Samples

sample	T (°C)	a	b	formula
LRC	25	3.44×10^{-3}	3.75×10^{-4}	$C_p = \frac{3.225 \times 10^{-4} \times P^{-0.14}}{3.44 \times 10^{-3} + 3.75 \times 10^{-4} \times P^{0.86}}$
	200	4.6×10^{-3}	2.73×10^{-4}	$C_p = \frac{2.539 \times 10^{-4} \times P^{-0.07}}{4.6 \times 10^{-3} + 2.73 \times 10^{-4} \times P^{0.93}}$
	400	1.07×10^{-2}	1.44×10^{-3}	$C_p = \frac{9.072 \times 10^{-4} \times P^{-0.37}}{0.0107 + 1.44 \times 10^{-3} \times P^{0.63}}$
	600	0.2043	5.82×10^{-3}	$C_p = \frac{1.979 \times 10^{-3} \times P^{-0.66}}{0.2043 + 5.82 \times 10^{-3} \times P^{0.34}}$
MRC	25	-3.12×10^{-2}	3.78×10^{-2}	$C_p = \frac{5.292 \times 10^{-3} \times P^{-0.86}}{-0.0312 + 0.0378 \times P^{0.14}}$
	200	-1.39×10^{-2}	2.71×10^{-2}	$C_p = \frac{4.607 \times 10^{-3} \times P^{-0.83}}{-0.0139 + 0.0271 \times P^{0.17}}$
	400	-3.45×10^{-2}	3.07×10^{-2}	$C_p = \frac{6.447 \times 10^{-3} \times P^{-0.79}}{-0.0345 + 0.0307 \times P^{0.21}}$
	600	-5.06×10^{-2}	6.07×10^{-2}	$C_p = \frac{5.376 \times 10^{-3} \times P^{-0.92}}{-0.0506 + 0.0607 \times P^{0.08}}$
HRC	25	0.3211	1.85×10^{-4}	$C_p = \frac{1.72 \times 10^{-4} \times P^{-0.07}}{0.3211 + 1.85 \times 10^{-4} \times P^{0.93}}$
	200	0.1969	1.78×10^{-4}	$C_p = \frac{1.655 \times 10^{-4} \times P^{-0.07}}{0.1969 + 1.78 \times 10^{-4} \times P^{0.93}}$
	400	0.336	3.65×10^{-4}	$C_p = \frac{2.956 \times 10^{-4} \times P^{-0.19}}{0.336 + 3.65 \times 10^{-4} \times P^{0.81}}$
	600	0.3594	2.6×10^{-4}	$C_p = \frac{2.236 \times 10^{-4} \times P^{-0.14}}{0.3594 + 2.6 \times 10^{-4} \times P^{0.86}}$

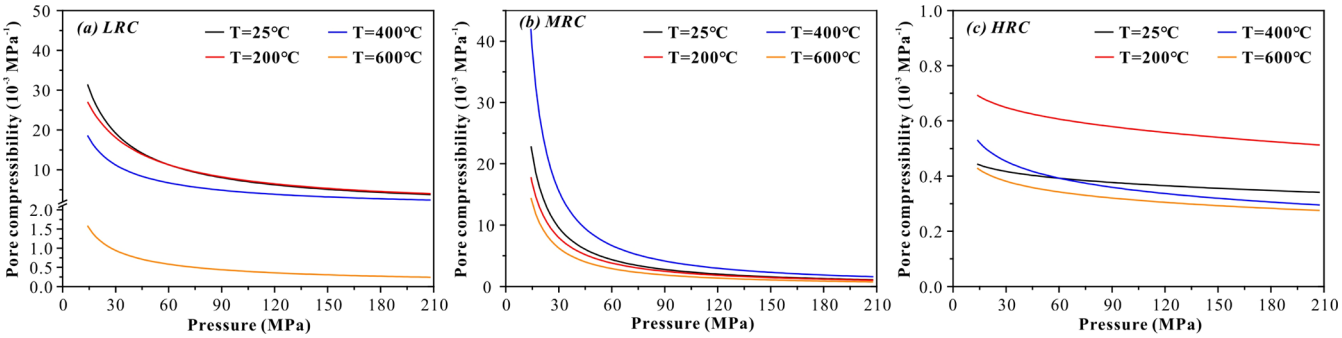

Figure 10. Pore compressibility variation discipline curves with a pressure of different rank coal samples.

(V_{mi}), V_p is generally replaced by V_{mi} in most instances.[23] As shown in Figure 9, when the mercury intrusion pressure ranges from 14.5 to 206 MPa (corresponding to a pore diameter interval of ~100−7.0 nm), a good linear correlation exists between mercury intrusion volume and the P^{D-3} value of coal samples under heat treatment, and the constants (a and b) can be obtained by fitting the MIP data.

Therefore, the pore compressibility of coals can be deduced from eqs 7 and 8

$$C_p = \frac{b(D-3)P^{D-4}}{a + bP^{D-3}} \tag{9}$$

Based on eq 9 and the fractal dimension D_{M2}, the pore compressibility of coal samples under heat treatments at different temperatures can be calculated by the corresponding formulas in Table 4, and their variation curves are plotted in Figure 10. For the LRC sample, the pore compressibility shows a decreasing trend as the temperature increases, corresponding to the interval of 3.82×10^{-3} to 3.09×10^{-2} MPa^{-1} for the LRC sample at 25 °C and 4.04×10^{-3} to 2.67×10^{-2} MPa^{-1} for the LRC sample at 200 °C, followed by 2.43×10^{-3} to 1.83×10^{-2} MPa^{-1} for the LRC sample at 400 °C and 2.45×10^{-4} to 1.55×10^{-3} MPa^{-1} for the LRC sample at 600 °C (Figure 10a). However, the pore compressibility is in the range of 9.43×10^{-4} to 4.03×10^{-2} MPa^{-1} for the MRC sample at 25−600 °C and has no obvious relationship with temperature (Figure 10b). As shown in Figure 10c, the pore compressibility of the HRC sample shows a rapidly increasing trend when the temperature increases from 25 °C (3.41×10^{-4} to 4.41×10^{-4} MPa^{-1}) to 200 °C (5.13×10^{-4} to 6.9×10^{-4} MPa^{-1}) and then decreases slowly as the temperature increases from 400 °C (2.96×10^{-4} to 5.24×10^{-4} MPa^{-1}) to 600 °C (2.76×10^{-4} to 4.25×10^{-4} MPa^{-1}). The above calculation results of the pore compressibility are in

https://dx.doi.org/10.1021/acs.energyfuels.0c00135
Energy Fuels 2020, 34, 3173−3187

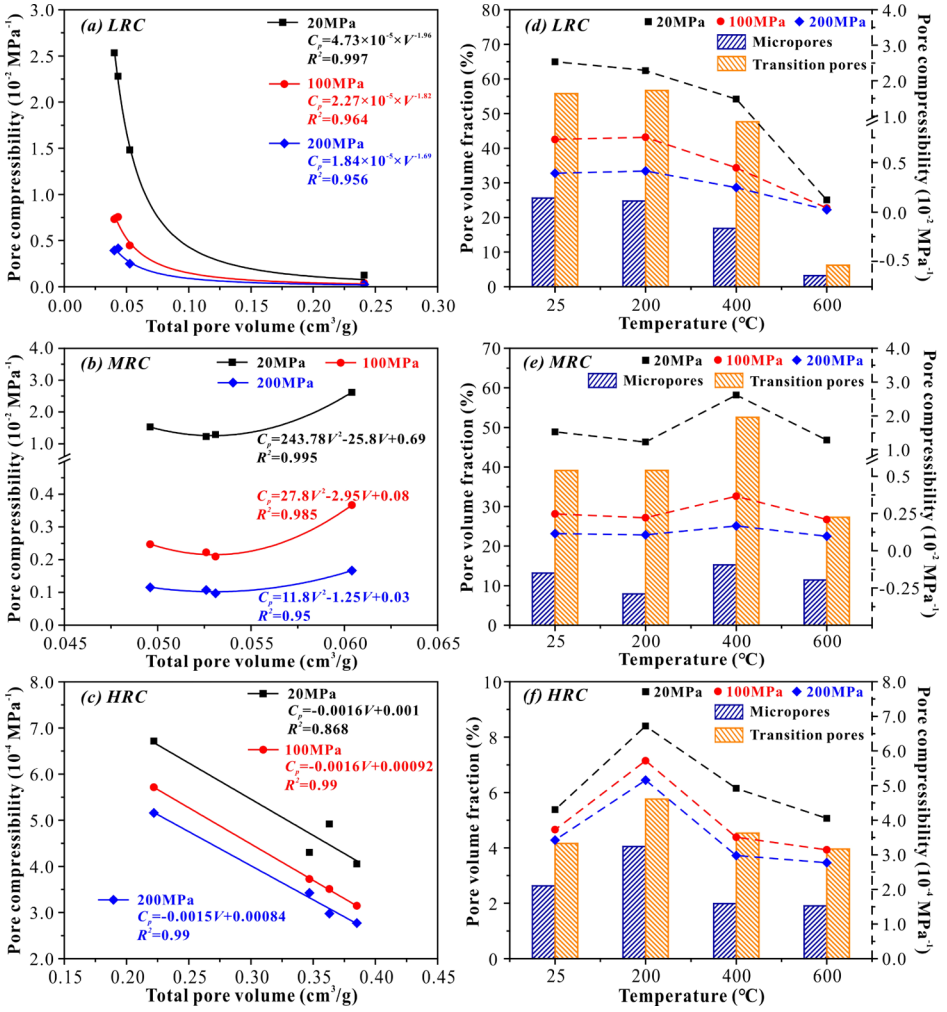

Figure 11. Relationship between pore structure (total pore volume and pore volume fraction) and pore compressibility of different rank coal samples.

accordance with the order of magnitude of the values obtained by other researchers.[23,43]

Moreover, the pore compressibility of coal samples basically presents a descending trend as the coalification degree increases (Figure 10), indicating that the lower metamorphic grade coal is more sensitive to pressure because of its more developed microporous structure. As shown in previous studies,[44,45] the matrix compressibility of coals is generally considered to be a constant in the high-pressure region with an order of magnitude of 10^{-5} to 10^{-4} MPa^{-1} and decreases as the coal rank increases. In comparison, the pore compressibility of coals varies dynamically with the mercury intrusion pressure. When the pressure is in the range of 14.5−206 MPa in this study, the pore compressibility values of the LRC sample (treated at 25, 200, and 400 °C) and MRC sample (treated at 25, 200, 400, and 600 °C) are completely in the range of 10^{-3} to 10^{-2} MPa^{-1} (Figure 10a,b), which far outweighs the matrix compressibility. This phenomenon indicates that the increase of mercury volume is mainly caused by the pore closure and collapse under high-pressure condition rather than the compaction of the coal matrix skeleton. However, the pore compressibility values of the LRC sample treated at 600 °C and the HRC sample treated at different temperatures are in close proximity to the matrix compressibility of coals (~10^{-4} MPa^{-1}) and slightly decrease as the experiment pressure increases (Figure 10a,c), which clearly suggests that the compaction of the coal matrix mainly contributes to the change of the mercury volume in these samples.

3.5. Impacts of Pore Structure on Pore Compressibility. Because the pore compressibility varies regularly as the pressure increases, taking the pore compressibility at 20, 100, and 200 MPa as an example, the effects of the total pore volume and the pore volume fraction of coals on the pore compressibility are studied in this work, as shown in Figure 11. An interesting phenomenon was discovered that the pore compressibility of each coal sample at the different pressures has the same variation tendency as the total pore volume. The pore compressibility of the LRC sample is related to the total pore volume in a negative power function with R^2 > 0.95 (Figure 11a), whereas the pore compressibility and total pore volume exhibits a slight "U" shape (a quadratic parabolic equation) relationship for the MRC sample and an obviously linear negative correlation for the HRC sample (Figure 11b,c). It can be inferred from the LRC and HRC samples that the increase of the total pore volume caused by the extensive development of macropores and microfractures during heat treatment may result in a decrease of pore compressibility. As mentioned above, the total pore volume of the MRC sample at elevated temperatures is mainly caused by the contribution of pores with diameter below 1000 nm. Meanwhile, massive adsorption pores are generated at 400 °C, which results in the pore compressibility values of the MRC sample treated at 25, 200, and 600 °C being

https://dx.doi.org/10.1021/acs.energyfuels.0c00135
Energy Fuels 2020, 34, 3173−3187

very close and then having a significant increase at 400 °C. Moreover, the pore compressibility values of the three coal samples show a remarkable positive correlation with the pore volume fraction of micropores and transition pores (Figure 11d,e,f). On the one hand, the main reason for this phenomenon is that more developed micropores and transition pores can provide a large amount of compressible space in the high-mercury intrusion pressure stage. On the other hand, the increase of the mercury volume resulting from the closure of closed or unconnected pores is much larger than that caused by the compression of the coal matrix skeleton. However, because the pore compressibility values of the HRC sample treated at different temperatures are close to the matrix compressibility coefficients of anthracite coals calculated by Shao et al.[28] (1.33×10^{-4} to 1.49×10^{-4} MPa^{-1}, $R_{o,m}$ = 2.99−3.12%), the compression of the coal matrix makes a significant contribution to the mercury intrusion volume of the HRC sample and should not be neglected. Additionally, Cai et al.[13] discussed the evolution of the submaceral composition at elevated treated temperatures for coals and its influence on the pore volume and distribution, which may essentially control the pore compressibility variation of coals. Therefore, complex changes in the pore structure and physical/chemical properties caused by metamorphism have a comprehensive influence on the compressibility of coals.

4. CONCLUSIONS

In this study, the thermal weight loss and gas generation, pore structure evolution, and pore compressibility of coals during heat treatment were investigated by combining TG−MS, N_2 adsorption/desorption, and MIP analysis. Meanwhile, the influence of the coal rank, temperature, and pore structure evolution on pore compressibility was discussed in detail. The following conclusions can be drawn

(1) The total thermal weight loss of the LRC sample is ∼40%, which is much greater than that of the MRC sample (∼15%) and the HRC sample (∼9%) during the heat treatment process (25−1200 °C). The macromolecular organic matter in the LRC and MRC samples begins to decompose into hydrocarbon gases (such as CH_4 and C_2H_4) at 350−600 °C, whereas only a small amount of hydrocarbon gas is generated in the HRC sample. Moreover, because of the decomposition of carbonate minerals and the polycondensation reaction, the production peaks of CO and CO_2 exist at 600−800 °C and are often accompanied by the generation of H_2 and H_2O.

(2) The surface morphology begins to soften at 200−350 °C and then exhibits the squamous structure or plastic deformation at ∼400 °C and changes to the spongy/honeycomb-shaped structure at 600 °C. Meanwhile, the pore structure and heterogeneity of the LRC and MRC samples treated at 25−200 °C change indistinctly because of the removal of moistures and partial volatiles, whereas the pore structure of the LRC and MRC samples has significantly changed, and its heterogeneity is reduced by the softening phenomenon and gas outburst at 400−600 °C. However, the pore structure and heterogeneity of the HRC sample show no obvious change as the temperature increases.

(3) The pore compressibility of the LRC sample shows a decreasing trend as the temperature increases (2.45×10^{-4} and 3.09×10^{-2} MPa^{-1}). Moreover, the pore compressibility of the MRC sample exhibits no obvious relationship with temperature (9.43×10^{-4} to 4.03×10^{-2} MPa^{-1} from 25 to 600 °C), whereas that of the HRC sample increases rapidly at first as the temperature increases to 200 °C and then decreases slowly as the temperature increases to 600 °C (2.76×10^{-4} to 6.9×10^{-4} MPa^{-1}). The pore compressibility presents a descending trend as the coalification degree increases and that also shows a strong positive correlation with the pore volume fraction of micropores and transition pores. Therefore, complex changes in the physical/chemical properties and pore structure have a comprehensive influence on the pore compressibility.

AUTHOR INFORMATION

Corresponding Author

Dameng Liu − *School of Energy Resources and Coal Reservoir Laboratory of National Engineering Research Center of CBM Development & Utilization, China University of Geosciences, Beijing 100083, China;* orcid.org/0000-0002-4688-074X; Phone: +86-10-82323971; Email: dmliu@cugb.edu.cn; Fax: +86-10-82326850

Authors

Zhentao Li − *State Key Laboratory of Organic Geochemistry, Guangzhou Institute of Geochemistry, Chinese Academy of Sciences, Guangzhou 510640, China; School of Energy Resources, China University of Geosciences, Beijing 100083, China*

Yidong Cai − *School of Energy Resources and Coal Reservoir Laboratory of National Engineering Research Center of CBM Development & Utilization, China University of Geosciences, Beijing 100083, China;* orcid.org/0000-0002-4915-5615

Guangyao Si − *School of Minerals and Energy Resources Engineering, University of New South Wales, Sydney, New South Wales 2052, Australia*

Yunpeng Wang − *State Key Laboratory of Organic Geochemistry, Guangzhou Institute of Geochemistry, Chinese Academy of Sciences, Guangzhou 510640, China*

Complete contact information is available at: https://pubs.acs.org/10.1021/acs.energyfuels.0c00135

Notes

The authors declare no competing financial interest.

ACKNOWLEDGMENTS

This research was funded by the National Natural Science Fund of China (grant nos. 41902165, 41830427, and 41772160), the Project funded by China Postdoctoral Science Foundation (grant no. 2018M643222), the International Postdoctoral Exchange Fellowship Program from China Postdoctoral Council (grant no. 20190070), Key Research and Development Projects of the Xinjiang Uygur Autonomous Region (grant no. 2017B03019-01), Strategic Priority Research Program of the Chinese Academy of Sciences (XDA14010103), and China National Major S&T Program (2017ZX05008-002-030).

REFERENCES

(1) Harpalani, S.; Prusty, B. K.; Dutta, P. Methane/CO_2 sorption modeling for coalbed methane production and CO_2 sequestration. *Energy Fuels* **2006**, *20*, 1591−1599.

(2) Mastalerz, M.; He, L.; Melnichenko, Y. B.; Rupp, J. A. Porosity of coal and shale: insights from gas adsorption and SANS/USANS techniques. *Energy Fuels* **2012**, *26*, 5109−5120.
(3) Li, Y.; Tang, D.; Elsworth, D.; Xu, H. Characterization of coalbed methane reservoirs at multiple length scales: A cross-section from southeastern Ordos Basin, China. *Energy Fuels* **2014**, *28*, 5587−5595.
(4) Li, Y.; Yang, J.; Pan, Z.; Meng, S.; Wang, K.; Niu, X. Unconventional natural gas accumulations in stacked deposits: a discussion of Upper Paleozoic coal-bearing strata in the east margin of the Ordos Basin, China. *Acta Geol. Sin* **2019**, *93*, 111−129.
(5) Pillalamarry, M.; Harpalani, S.; Liu, S. Gas diffusion behavior of coal and its impact on production from coalbed methane reservoirs. *Int. J. Coal Geol.* **2011**, *86*, 342−348.
(6) Shi, J.-Q.; Durucan, S. Gas storage and flow in coalbed reservoirs: implementation of a bidisperse pore model for gas diffusion in coal matrix. *SPE Reservoir Eval. Eng.* **2005**, *8*, 169−175.
(7) Fu, H.; Tang, D.; Xu, H.; Tao, S.; Xu, T.; Chen, B.; Yin, Z. Abrupt changes in reservoir properties of low-rank coal and its control factors for methane adsorbability. *Energy Fuels* **2016**, *30*, 2084−2094.
(8) Takahashi, K. U.; Suzuki, N.; Saito, H. Compositional and isotopic changes in expelled and residual gases during anhydrous closed-system pyrolysis of hydrogen-rich Eocene subbituminous coal. *Int. J. Coal Geol.* **2014**, *127*, 14−23.
(9) Kelly, K. E.; Wang, D.; Hradisky, M.; Silcox, G. D.; Smith, P. J.; Eddings, E. G.; Pershing, D. W. Underground coal thermal treatment as a potential low-carbon energy source. *Fuel Process. Technol.* **2016**, *144*, 8−19.
(10) Akbarzadeh, H.; Chalaturnyk, R. J. Structural changes in coal at elevated temperature pertinent to underground coal gasification: A review. *Int. J. Coal Geol.* **2014**, *131*, 126−146.
(11) Hosseini, T.; De Girolamo, A.; Zhang, L. Energy evaluation and techno-economic analysis of low-rank coal (Victorian brown coal) utilization for the production of multi-products in a drying-pyrolysis process. *Energy Fuels* **2018**, *32*, 3211−3224.
(12) Liu, H.; Liu, S.; Chen, F.; Zhao, J.; Qi, K.; Yao, H. Mathematical modeling of the underground coal gasification process in one gasification cycle. *Energy Fuels* **2019**, *33*, 979−989.
(13) Cai, Y.-D.; Liu, D.-M.; Liu, Z.-H.; Zhou, Y.-F.; Che, Y. Evolution of pore structure, submaceral composition and produced gases of two Chinese coals during thermal treatment. *Fuel Process. Technol.* **2017**, *156*, 298−309.
(14) Clarkson, C. R.; Bustin, R. M. The effect of pore structure and gas pressure upon the transport properties of coal: a laboratory and modeling study: 1. Isotherms and pore volume distributions. *Fuel* **1999**, *78*, 1333−1344.
(15) Hodot, B. B. *Outburst of Coal and Coalbed Gas*; China Industry Press: Beijing, 1966, pp 23−35.
(16) Li, Y.; Zhang, C.; Tang, D.; Gan, Q.; Niu, X.; Wang, K.; Shen, R. Coal pore size distributions controlled by the coalification process: An experimental study of coals from the Junggar, Ordos and Qinshui basins in China. *Fuel* **2017**, *206*, 352−363.
(17) Bustin, R. M.; Guo, Y. Abrupt changes (jumps) in reflectance values and chemical compositions of artificial charcoals and inertinite in coals. *Int. J. Coal Geol.* **1999**, *38*, 237−260.
(18) Lorenz, H.; Carrea, E.; Tamura, M.; Haas, J. The role of char surface structure development in pulverized fuel combustion. *Fuel* **2000**, *79*, 1161−1172.
(19) Yu, Y.; Liang, W.; Hu, Y.; Meng, Q. Study of micro-pores development in lean coal with temperature. *Int. J. Rock Mech. Min. Sci.* **2012**, *51*, 91−96.
(20) Yang, Y.; Zheng, K.; Li, Z.; Li, Z.; Si, L.; Hou, S.; Duan, Y. Experimental study on pore-fracture evolution law in the thermal damage process of coal. *Int. J. Rock Mech. Min. Sci.* **2019**, *116*, 13−24.
(21) Li, Z.; Liu, D.; Cai, Y.; Yao, Y.; Wang, H. Pore structure and compressibility of coal matrix with elevated temperatures by mercury intrusion porosimetry. *Energy Explor. Exploit.* **2015**, *33*, 809−826.
(22) Friesen, W.; Mikula, R. Mercury porosimetry of coals: Pore volume distribution and compressibility. *Fuel* **1988**, *67*, 1516−1520.
(23) Qu, Z.; Wang, G. G. X.; Jiang, B.; Rudolph, V.; Dou, X.; Li, M. Experimental study on the porous structure and compressibility of tectonized coals. *Energy Fuels* **2010**, *24*, 2964−2973.
(24) Okolo, G. N.; Everson, R. C.; Neomagus, H. W. J. P.; Roberts, M. J.; Sakurovs, R. Comparing the porosity and surface areas of coal as measured by gas adsorption, mercury intrusion and SAXS techniques. *Fuel* **2015**, *141*, 293−304.
(25) Raza, S. S.; Ge, L.; Rufford, T. E.; Chen, Z.; Rudolph, V. Anisotropic coal permeability estimation by determining cleat compressibility using mercury intrusion porosimetry and stress-strain measurements. *Int. J. Coal Geol.* **2019**, *205*, 75−86.
(26) Li, X.; Fu, X.; Ranjith, P. G.; Xu, J. Stress sensitivity of medium- and high volatile bituminous coal: An experimental study based on nuclear magnetic resonance and permeability-porosity tests. *J. Petrol. Sci. Eng.* **2019**, *172*, 889−910.
(27) Yu, S.; Jiang, B.; Shao, P.; Wu, J. H. Matrix compression and multifractal characterization for tectonically deformed coals by Hg porosimetry. *Fuel* **2018**, *211*, 661−675.
(28) Shao, P.; Wang, X.; Song, Y.; Li, Y. Study on the characteristics of matrix compressibility and its influence factors for different rank coals. *J. Nat. Gas Sci. Eng.* **2018**, *56*, 93−106.
(29) Akbarzadeh, H.; Chalaturnyk, R. J. Coupled fluid-thermal-mechanical analyses of a deep underground coal gasification cavity. *J. Archit. Civil Eng.* **2013**, *1*, 1−14.
(30) Li, Y.; Wang, Z.; Pan, Z.; Niu, X.; Yu, Y.; Meng, S. Pore structure and its fractal dimensions of transitional shale: A cross-section from east margin of the Ordos Basin, China. *Fuel* **2019**, *241*, 417−431.
(31) Washburn, E. W. The dynamics of capillary flow. *Phys. Rev.* **1921**, *17*, 273−283.
(32) Yao, Y.; Liu, D.; Tang, D.; Tang, S.; Huang, W. Fractal characterization of adsorption-pores of coals from North China: an investigation on CH_4 adsorption capacity of coals. *Int. J. Coal Geol.* **2008**, *73*, 27−42.
(33) Friesen, W. I.; Mikula, R. J. Fractal dimensions of coal particles. *J. Colloid Interface Sci.* **1987**, *120*, 263−271.
(34) Mahamud, M.; López, Ó.; Pis, J. J.; Pajares, J. A. Textural characterization of coals using fractal analysis. *Fuel Process. Technol.* **2003**, *81*, 127−142.
(35) Wang, M.; Li, Z.; Huang, W.; Yang, J.; Xue, H. Coal pyrolysis characteristics by TG-MS and its late gas generation potential. *Fuel* **2015**, *156*, 243−253.
(36) Solomon, P. R.; Serio, M. A.; Despande, G. V.; Kroo, E. Cross-linking reactions during coal conversion. *Energy Fuels* **1990**, *4*, 42−54.
(37) Zeng, F.-G.; Jia, J. B. Reaction types and kinetics of methane generation from Huolinhe lignite pyrolysis by TG/MS experiment and quantum chemical calculations. *Acta Phys. Sin.* **2009**, *25*, 1117−1124.
(38) Gneshin, K. W.; Krumm, R. L.; Eddings, E. G. Porosity and structure evolution during coal pyrolysis in large particles at very slow heating rates. *Energy Fuels* **2015**, *29*, 1574−1589.
(39) Wang, Y.; Zhao, Y. S.; Feng, Z. Z. Study of evolution characteristics of pore structure during flame coal pyrolysis. *Chin. J. Rock Mech. Eng.* **2010**, *29*, 1859−1866.
(40) Yao, Y. B.; Liu, D. M. *Advanced Reservoir Quantitative Characterization and Comprehensive Evaluation Model of Coalbed Methane Reservoirs*; Geological Publishing House: Beijing; 2013.
(41) Zhang, S.; Tang, S.; Zhang, J.; Pan, Z. Pore structure characteristics of China sapropelic coal and their development influence factors. *J. Nat. Gas Sci. Eng.* **2018**, *53*, 370−384.
(42) Li, Y.-H.; Lu, G. Q.; Rudolph, V. Compressibility and fractal dimension of fine coal particles in relation to pore structure characterisation using mercury porosimetry. *Part. Part. Syst. Char.* **1999**, *16*, 25−31.
(43) Xu, L.; Liu, C.; Xian, X.; Zhang, D. Compressibility of coal matter and coal pore. *Colloids Surf., A* **1999**, *157*, 219−222.
(44) Guo, X.; Yao, Y.; Liu, D. Characteristics of coal matrix compressibility: an investigation by mercury intrusion porosimetry. *Energy Fuels* **2014**, *28*, 3673−3678.

https://dx.doi.org/10.1021/acs.energyfuels.0c00135
Energy Fuels 2020, 34, 3173−3187

(45) Cai, Y.; Li, Q.; Liu, D.; Zhou, Y.; Lv, D. Insights into matrix compressibility of coals by mercury intrusion porosimetry and N_2 adsorption. *Int. J. Coal Geol.* **2018**, *200*, 199−212.

https://dx.doi.org/10.1021/acs.energyfuels.0c00135
Energy Fuels 2020, 34, 3173−3187